# Acoustic Emission Signals versus Propagation Direction for Hybrid Composite Layup with Large Stiffness Differences versus Direction

Marvin A. HAMSTAD *, Markus G. R. SAUSE **
* University of Denver, Daniel Felix Ritchie School of Engineering and Computer Science, Denver, CO, USA
** University of Augsburg, Augsburg, Germany

**Abstract.** In the cylindrical section, a composite pressure vessel (COPV) has nearly twice as many fibers in the hoop direction as in the axial direction. Thus, the COPV has a significant difference in the stiffness (bending and in-plane) in these two perpendicular directions. For acoustic emission (AE) monitoring, these stiffness differences can significantly change the AE waves as a function of the propagation direction. In addition, the primary direction of the release of stresses from fracture events (e.g., fiber fracture and transverse cracking) relative to the local fiber direction also is expected to be a factor in the observed AE signals. The situation is typically further complicated for COPVs by the presence of a thin metal liner. To begin a systematic study of the effect of stiffness changes on the AE signals versus propagation direction, the variables of source depth and source orientation were examined by finite element modeling. In-plane dipole sources in the two principal fiber directions at different source depths were used for a 0°/90° layup carbon fiber/polymer with twice the number of fibers in the 90° (hoop) direction as in the 0° (axial) direction. The composite was coupled to a thin aluminum liner. The out-of-plane displacement signals were obtained for different propagation angles at 60 mm from the source. Choi-Williams distributions (CWDs) (frequency/time intensity) were obtained to show correspondence to group velocity curves. The peak amplitudes and the CWD (magnitudes at fixed frequencies) of the fundamental flexural mode versus the propagation direction were obtained as a function of the source depth and orientation. The changes of the amplitudes of the flexural mode the AE signals with propagation direction were found to be significant for the variables of source depth and orientation.

## 1. Introduction

A key advantage when structures are fabricated from fiber composites is the ability to align more expensive high strength fibers in the directions where the applied stresses are high and fewer in the directions of low applied stresses. This situation is present in the cylindrical portion of a cylindrical composite pressure vessel (COPV), where stresses due to the internal pressure are twice as large in the hoop direction as in the axial direction. Often a significant fraction of the extra layers of fibers aligned in the hoop direction are placed on the outer portion of the cylindrical section wall with the predominately axially-oriented fibers in the layers below. The net result is a significant difference in

the stiffness (bending and in-plane) of the resulting composite in these two perpendicular directions along with significant changes in stiffness at the in-between angles. During acoustic emission (AE) monitoring of such COPVs, the differences in the character and amplitude of the AE waves as a function of the propagation direction from the source to the sensor potentially can be expected to be significant. Some of these differences are clearly present in the well-known changes in group velocities versus propagation direction in anisotropic plates. In addition, the dominant direction of the release of stresses from fracture events relative to the composite layer (hoop or axial), in which it operates, may also be a significant factor in the observed AE signals. For example, the generation from a transverse crack (to the local fiber direction) in the matrix would be expected to locally release a dominant portion of its stored energy in a low stiffness direction, while a fiber fracture source would be expected to locally release a dominant portion of its stored energy in a high stiffness direction. Additionally, this situation can be complicated for COPVs by the presence of a thin metal liner on the inside of the composite shell.

With the above in mind, for the AE practitioner and researcher there are a number of questions that can arise relative to monitoring cylindrical COPVs. For example, how does the peak signal amplitude change versus propagation direction? Often for economic reason only a few sensors are used. Thus, the sensors may not be ideally located at the best propagation angles from the different sources, with the result that some AE events are not detected or too few sensors generate sufficient amplitudes to perform source location. In the case of the use of resonant sensors, one might ask, is the frequency response of the sensor sensitive to the frequencies carried in the possible range of propagation directions? The researcher attempting to do source type determination might ask, do the sensors in use have a sufficiently wide range of similar frequency response to be able to properly characterize the frequencies in the wave arriving from different propagation directions relative to different source types, depths or orientations?

The purpose of this work is to begin a systematic study for cylindrical COPVs of the effect of propagation direction on the AE signals in relation to source depth (physical depth and layer in which the source operates) and source orientation in the layer. An earlier study was only partially focused on COPVs [1]. The results of the current study are expected to provide some initial answers to the above questions. This work takes advantage of finite element modeling (FEM), which was used in a previous examination of AE signals as a function of direction of propagation versus source depth in an isotropic material plate [2]. The primary advantage of the use of FEM is that precise control of source characteristics (such as rise time and source orientation), source location and propagation distance/direction is possible. In addition, the AE signals are those from a perfectly flat-with-frequency pseudo sensor. Thus, it is possible to obtain precise data as a function of the listed variables. In the case of experimental data from undamaged cylindrical COPVs, it is not practical to obtain such systematic data. For example, the source depth through the thickness is likely unknown, and, due to the random location of sources, it is not likely that AE signals could be obtained at a fixed propagation distance from each source at multiple propagation angles so as to obtain propagation angle results independent of the propagation distance and the associated dispersion and geometric spreading. In the current study, the presence of a fluid in contact with the inside of the vessel is not considered. An initial examination of this situation relative to a hydro test has been recently completed [3].

## 2. AE Source and Finite Element Conditions

Dipole sources in the two principal fiber directions at different source depths in a hybrid plate were modeled for the more extreme case of a 0°/90° layup with twice the number of fibers in the 90° (hoop) direction as in the 0° (axial or longitudinal) direction. Further, the additionally extreme case was examined where all the 90° fibers are in the outer layers with the 0° layers below. Finally, a thin aluminum alloy liner was at the bottom of the plate. As a relevant aside, a cylindrical metal vessel with all 90° hoop wraps, also has large stiffness changes in the two primary directions. A carbon fiber/polymer was selected as the composite material. The thickness of the resulting hybrid composite going from the top (where AE sensors would be placed) to the bottom was: 2 mm with 90° fibers, 1 mm with 0° fibers and 1.3 mm aluminum liner (total thickness 4.3 mm). The properties of these materials are given in table 1. The modeling domain was a quarter-circle plate with a radius

**Table 1** Elastic properties used for FEM modeling and dispersion calculations

| Property | $AlMg_3$ | T800/913 |
|---|---|---|
| Density [$kg/m^3$] | 2660 | 1550 |
| Elastic Modulus [GPa] | 70.0 | $C_{11}$ = 154.0, $C_{23}$ = 5.2, $C_{22}$ = $C_{33}$ = 9.5, $C_{44}$ = 2.5<br>$C_{22}$ = $C_{33}$ = 9.5, $C_{44}$ = 2.5, $C_{12}$ = $C_{13}$ = 3.7, $C_{55}$ = $C_{66}$ = 4.2 |
| Poisson ratio | 0.33 | - |

of 160 mm using symmetry conditions at 0° and 90°. The source was a dipole (modeled as monopole using symmetry conditions) located near the origin in this domain. To avoid significant reflections from the radial edge reaching the 60 mm observation distance a low-reflecting boundary condition as defined in [1] was used. Figure 1 shows the domain, coordinate axis directions and origin. The in-plane sources were located at five different depths indicated by the distance from the bottom of the aluminum (z-axis origin). Two were in the 0° layer (at 1.5 and 2.2 mm) and three in the 90° layer (at 2.5, 3.2 and 4.1 mm). In the region of the source, a tetrahedral mesh was used for a "sub-square" of side dimension 10 mm, as shown in figure 1. Away from the source region, a hexagonal mesh was used. For all regions a maximum edge length of 1 mm was chosen for the mesh elements. The computational time step chosen for the analysis was 0.1 µs. In addition, a check that verified the convergence of the results (waveform and frequency spectrum) was made by comparison of the results with a run with maximum edge length of 0.5 mm and computational time step of 0.05 µs.

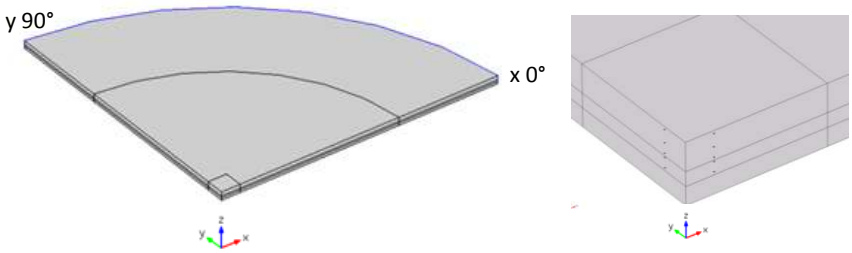


**Figure 1.** Domain of FEM modeling. Radii show 60 mm propagation distance and 160 mm outer radius (blue, low reflecting boundary). Small dots near the origin (right figure) show the source locations. Note z axis zero at bottom of plate.

The source forces were applied to single nodes. For a source with force in the y-axis direction (called a YDP) the (x, y) coordinates of the source were respectively (0, 2) mm. And for the force in the x-axis direction (called a XDP) the corresponding values were (2, 0) mm. It is important to note that applicability of the dipole size of 4 mm was checked by a run with a dipole size of 0.6 mm. This run showed nearly identical results as a function of the propagation angle. The source function had a linear rise in time to 3 N in 1 µs. Out-of-plane displacement signals at nodal points on the top and bottom (aluminum) surfaces were obtained at five degree increments in the propagation angle from 0° to 90° for a signal length of 120 µs (0 µs at the start of the force function). The 60 mm propagation distance was sufficient to allow the development of Lamb-type waves. Signal analysis was initially done on unfiltered data. Subsequently, different frequency filters were applied either to better represent the frequency range present in existing AE sensors or to highlight certain modal regions. The data set was large with 190 waveforms each for the top and bottom surfaces. Also, each different filter created a new set of 190 or 380 waveforms.

## 3. Initial Analysis of AE Signals

To provide some background for the analysis and to further demonstrate the validity of the FEM generated signals, group velocities for three relevant modes (A0, S0 and S1) as a function of frequency were calculated for the hybrid plate [4]. Figure 2 shows top-surface and unfiltered displacement signals and Choi Williams distributions (CWD) [5, 6] (parameters were default except frequency band = 1.22 kHz) results with superimposed group velocity curves for three diverse

waveform cases that illustrate the "fit" of the group velocity results for propagation directions of 0°, 45° and 90°. It is clear that the CWD results match very well with the group velocity curves. This match provides an independent verification of the FEM calculated results. Clearly, there are some significant differences in the group velocity curves with propagation direction. As the propagation angle increases from 0° to 90°, the time period of potential activity of the S0 mode consistently increases. For the higher frequency region (above about 50 kHz) of the A0 mode, as the propagation angle increases (0° to 90°), the arrival time difference between the first and last portion occurs over a shorter range of time. On the other hand, the time period of potential activity of the higher frequency region of the S1 mode changes in a non-consistent fashion as the angle of propagation increases. Also, it is evident that the signal intensity is predominately in the low frequency portion of the A0 mode, high frequency portion of the S0 mode and a high frequency portion of the S1 mode. As will be discussed later, this characterization of the intensity of the signals is similar for a majority of the waveforms. Due to the overlap of the higher frequency portions of the S0 and S1 modes at certain angles of propagation (for example at 90°) and the fact that both are symmetric modes, it is not always possible to distinguish between them by comparison with the signals from the bottom surface. Also, comparisons of the top and bottom surface signals did not exhibit the expected similarities in the low frequency portion of the S0 mode. The reason was likely due to guided wave modes that exist within one or both the top and bottom layers of the plate. Such guided waves within a layer were also reported in the earlier work [1].

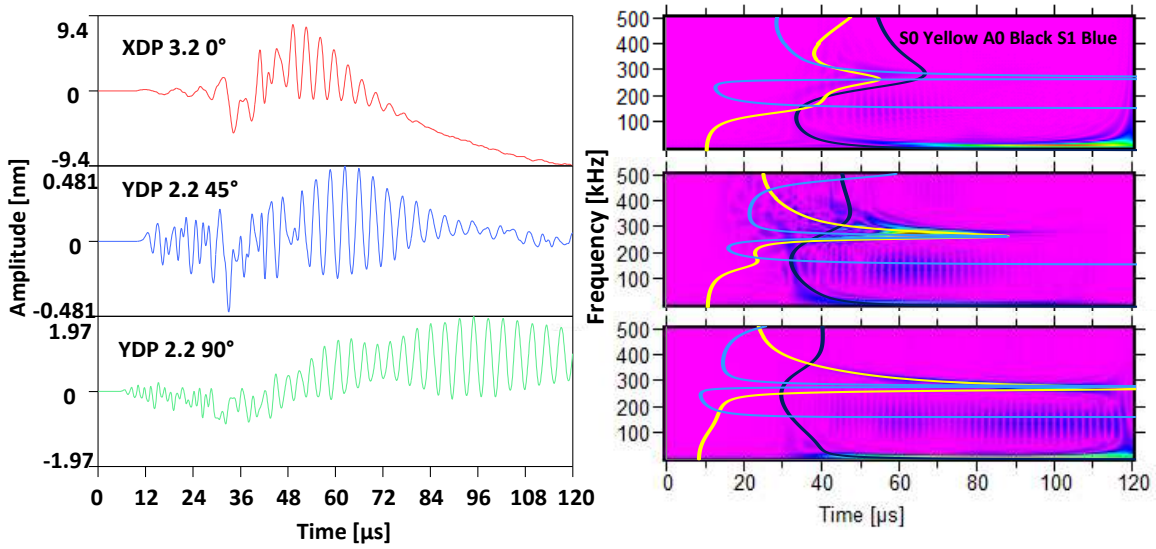


**Figure 2.** Three different modeled signals (unfiltered) and their CWD results (to the right) at the indicated propagation angles, source directions and source depths showing fit of group velocity curves converted to frequency versus time to propagate 60 mm.

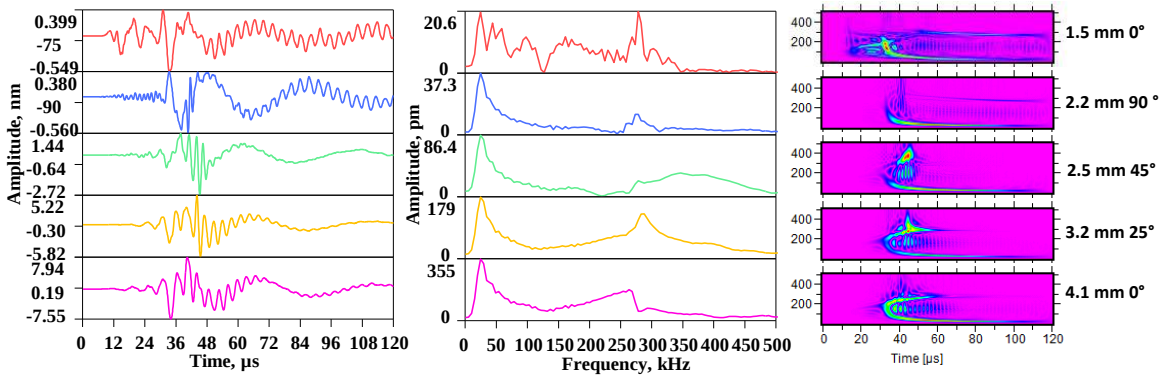


**Figure 3.** Range of signals of XDP cases for 20 kHz HP data. Waveform, FFT and CWD (0 to 500 kHz). Depths and angles of propagation as shown for rows.

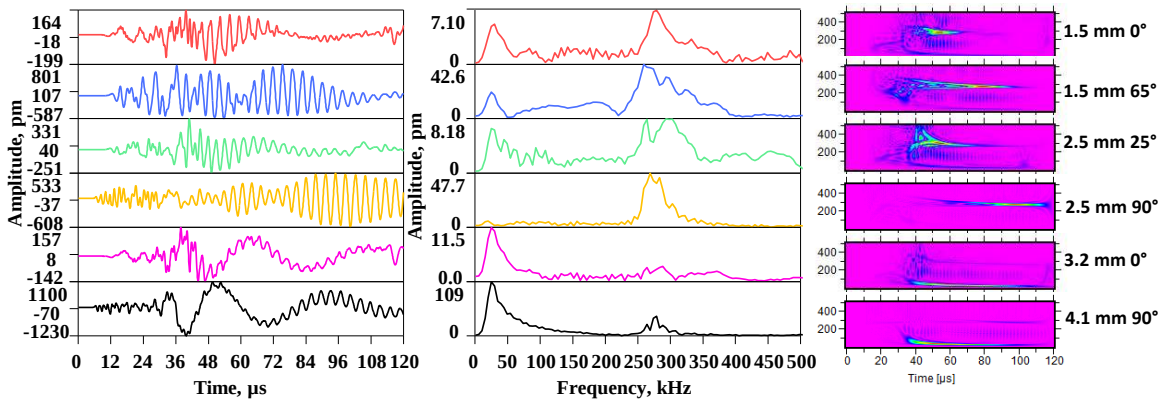


**Figure 4.** Range of signals of YDP cases for 20 kHz HP data. Waveform, FFT and CWD (0 to 500 kHz). Depths and angles of propagation shown for rows.

## 4. Analysis of Wideband Filtered AE Signals

### 4.1 Filtering

To begin to develop analysis more relevant to the demonstrated bandwidth of experimentally used AE sensors, a high-pass (HP) 6 pole 20 kHz Butterworth filter was applied to the data. Figures 3 and 4 show respectively for XDPs and YDPs a range of top surface waveforms (here and all subsequent results), fast Fourier transform (FFT) results and CWD results as a function of source direction, depth and propagation direction. These cases, chosen to effectively span the range of most of the waveforms in the database, provide evidence that there are two primary frequency ranges of signal intensity, a low frequency region and a higher frequency region. These figures imply, that for AE monitoring of such a composite to fully characterize the amplitude and frequency content of the waves requires sensors having both low frequency response as well as higher frequency equivalent amplitude response. These figures also show that for a majority of the waveforms the examination of the amplitudes of the most dominant modal regions could be done with specific filtering (high-pass [HP] and low-pass [LP]) chosen to isolate either the lower frequency region of the A0 mode or the high frequency region of the S0 and S1 modes.

### 4.2 Background relative to determination of propagation direction effects

From the initiation of the of the source until the AE waves reach the 60 mm propagation distance, there are several processes that are potentially present. First, the dynamic displacements created by the source forces interact with the stiffness properties of the local material properties. Further, the examination of the total static stored strain energy (static displacement field due to a 3N force at the loaded node) from the dipoles located near an interface (e.g. 2.2 mm depth) showed that up to about 10 % of the stored energy would be in the adjacent layer. Second, as the waves propagate further, the formation of Lamb-type guided waves begins and proceeds so that at the 60 mm distance the waves can involve the total plate thickness, and they have the characteristics of the symmetric and anti-symmetric modes that reflect the dynamic stiffness properties of the full plate thickness. In the present study of the propagation direction features, the focus is on the characteristics of the full thickness mode-based signals at the 60 mm observation point. In the real world of composite COPVs, the presence of a matrix material with viscoelastic properties implies that higher frequencies will attenuate more rapidly with distance than lower frequencies. Further, in most applications of AE monitoring of such COPVs, the sensor array is such that other than possibly the first-hit sensor, the propagation distances are typically greater than 60 mm. Hence, there is additional loss of higher frequencies due to material attenuation. Thus, based on these facts and also observations on real AE signals from COPVs, where often the flexural mode is dominant, for the current initial analysis of the effect of the propagation direction, the focus is on the flexural mode

isolated by a 20 kHz HP filter (6 pole, Butterworth) followed by a 150 kHz LP filter (8 pole, Butterworth).

### 4.3 Peak amplitude of flexural mode and its dependence on propagation angle

After applying the above filter, the waveforms had clear flexural and extensional mode regions. Figure 5 demonstrates a correlation of the corrected peak flexural mode amplitude in the source direction versus the absolute difference in distance through the thickness from the source depth to the mid-plane (at z = 2.15 mm). The amplitude correction was done by dividing the peak flexural amplitude for each case by the total strain energy from the static displacement field for that case. This correction was necessary to compensate for the difference in source strength due to the change in stiffness for sources parallel compared to perpendicular to the local fiber direction. The general trend is an increase in the amplitude as the difference from the mid-plane increases. This amplitude change can be several dB or more for the same source type. These results are similar to the behavior of the peak amplitude of the flexural mode as a function of source depth relative to the mid-plane of a plate of isotropic material [7]. Due to the complex layup and the fact of interfaces near the depth of the dipole sources, there are some deviations from the simple correlation as is present for an isotropic plate. A current analysis [8] of the data in reference 7, showed a very near linear dependence on the difference between the source depth and the mid-plane for the isotropic case.

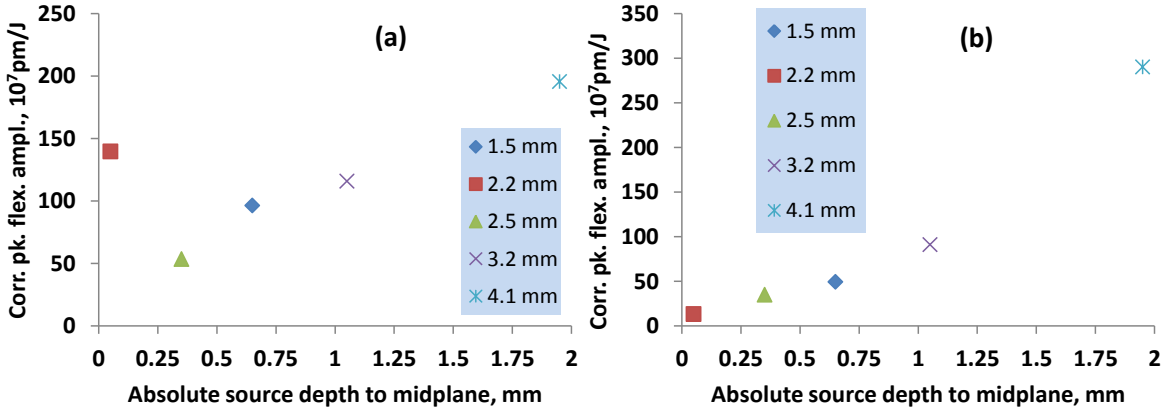


**Figure 5.** Corrected peak flexural mode amplitude in the source direction versus the absolute distance from the source depth to the mid-plane of the hybrid at the indicated source depths. XDPs (a) and YDPs (b).

Since figure 5, only provides the results in the source direction, figure 6(a) shows the normalized peak amplitude of the flexural mode versus all the angles from the source direction (0°) for the XDPs at different source depths, and figure 6(b) shows the same results for the YDPs (from the source direction 90°). In this figure, the normalization of the peak amplitude for each case was done by the peak flexural amplitude of the signal propagating in the source direction (thus it was not necessary to correct for the stiffness differences as was done for figure 5). The general loss of amplitude with increasing angle demonstrated in these figures is expected based on the analytical results for dipoles in isotropic materials [9]. For the XDPs the amplitude changes with increasing angle follows a regular pattern of most falloff for the 4.1 mm depth to least for 1.5 mm. This regular pattern is not the case for the YDPs. When the rate of falloff from 0° to about 25° is compared for the XDPs versus the YDPs, it is observed to be significantly larger for the YDPs. The maximum normalized amplitude loss for the XDPs is about 14 dB (4.1 mm depth) and for the YDPs it is about 20 dB (1.5 and 4.1 mm). Changing the HP frequency from 10, to 20 to 40 kHz prior to the 150 kHz LP filter showed that the general pattern of falloff with increasing angle from the source direction was preserved, but there are some small changes that indicate sensor response and/or filtering can change the detected amplitudes. The results in figure 6 along with those in figure 5 indicate that using peak amplitudes to determine AE sources types could create significant errors even in the ideal case of equal propagation distances from the source to the sensors due to the propagation direction differences with the variables of source direction and source depth. In addition, the changes shown in figure 6 are in contrast to those for dipoles in an isotropic material plate. In the

isotropic plate the normalized peak flexural amplitude was found to decrease in proportion to the square of the cosine of the angle from the source direction for all depths of the dipole [8, 9].

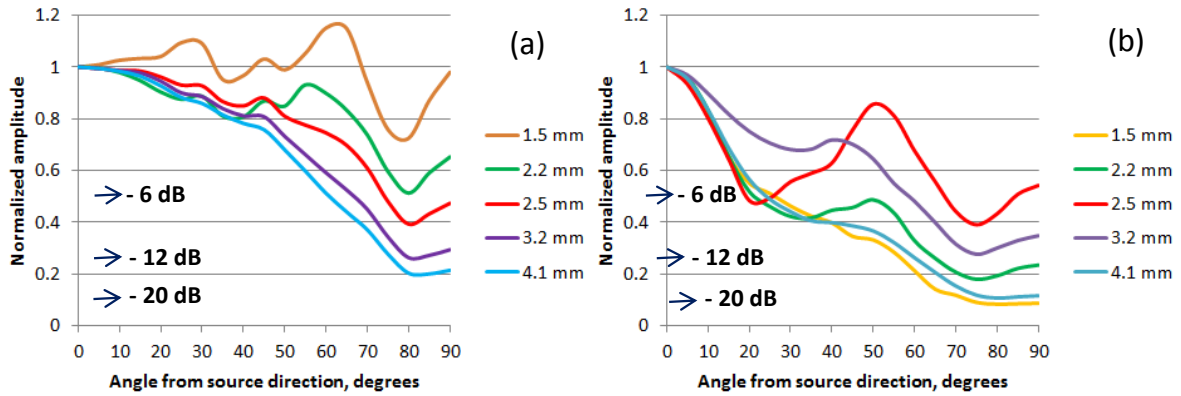


**Figure 6.** Normalized peak amplitude of flexural mode of XDPs (a) and YDPs (b) versus angle of propagation from source direction (0°) for data filtered 20 kHz HP followed by 150 kHz LP.

## 5. CWD magnitude at a Fixed Frequency of the Flexural mode

After examining the frequency of the peak magnitude of the CWD for the flexural mode for a series of XDP cases of source depth and propagation angle, it was determined the CWD magnitude at 40 kHz was a suitable frequency to evaluate the CWD magnitude versus source depth and propagation angle. Since the CWD magnitudes are proportional to energy, to be able to compare these results with the amplitudes of figure 6, the square root of the CWD magnitudes were used (denoted by SRCWD). The normalized (by the SRCWD magnitude in the source direction for each case) results are shown in figure 7(a) for 40 kHz for the XDP signals after they had been filtered at 20 kHz HP followed by 150 kHz LP. The results demonstrated a systematic change as a function of source depth with the largest "falloff" with increasing angle being for 4.1 mm and the least "falloff" being for 1.5 mm. This is the same "falloff" ordering as for the peak amplitude in figure 6(a). It is interesting that the 1.5 mm case has the largest changes. The "falloff" or "rise" for the other depths are less dramatic, but the angles from the source direction of fall and rise are about the same as the 1.5 mm case, with smaller deviations as the depth increases. In general, if the XDP SRCWD results are compared to the normalized peak flex amplitude (figure 5(a)), there are some similar characteristics in the shape of the fall and rise of the amplitude versus angle regions.

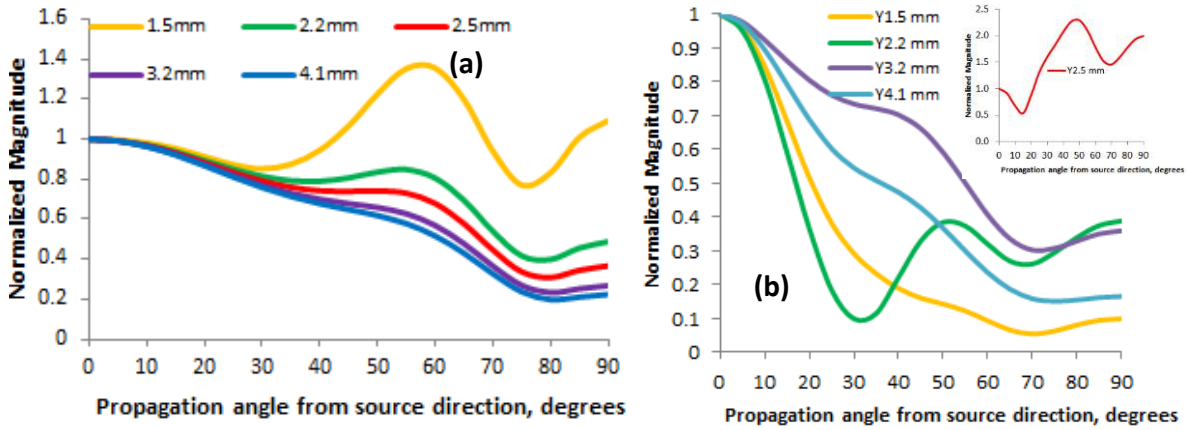


**Figure 7.** Normalized SRCWD peak magnitudes for 40 kHz for XDPs (a) and 27 kHz for YDPs (b). Filtered data from 20 kHz HP and by 150 kHz LP. Inset in (b), due to large magnitude of 2.5 mm case.

For the YDP case, the survey of the CWD peak frequency of the flexural mode did not result in being able to use 40 kHz as the fixed frequency to characterize the flexural mode. Instead to be able to reliably measure the peak CWD magnitude of the flexural mode it was convenient to

use 27 kHz. The results for the SRCWD are shown in figure 7(b). As was the case in figure 6(b) for the normalized peak flexural mode amplitude of the YDP, the 2.5 mm case had a normalized peak SRCWD magnitude at a similar angle from the source direction at about 50°. In this SRCWD case, the peak magnitude here was well above that in the source direction by a factor of about 2.2 times (see figure inset). Again the results in figure 7 are in sharp contrast to previous isotropic plate results. In the isotropic case the wavelet transform (which is proportional to amplitude) normalized magnitude at a fixed frequency in the flexural mode had the same dependence versus the propagation angle from the source for all dipole source depths [2].

## 6. Conclusions

This study provides the primary features to be expected in the AE signals in different propagation directions in the cylindrical section of metal-lined COPVs relative to the effects of different source orientation and depth. The details for other cases will depend on particular layups and thicknesses for hybrids with large stiffness changes in layers and directions. First, for the current hybrid composite there are significant contrasts relative to the AE signal behavior from dipole sources at different depths and propagation directions in an isotropic material plate. In particular: (i) the frequency content and waveform character experience large changes as a function of propagation direction and source direction and depth as shown in figures 3 and 4; (ii) the peak amplitude of the flexural mode in the source direction increases as the absolute difference in the depth of the source versus the mid-plane increases, but for the hybrid it is not the linear dependence for an isotropic plate.; (iii) the normalized peak amplitude and the normalized magnitude of the SRCWD (at a fixed frequency) of the flexural mode versus propagation direction, which did not change with the source depth for a isotropic plate, now vary for each source depth and source direction; (iv) the variation for the flexural mode peak amplitude and SRCWD magnitude with propagation direction indicates that there are preferred directions with smaller amplitude losses and non-preferred directions with larger amplitude losses. Second, from a practical point of view, since generally the propagation directions from the sources to the sensors are not known before a test, it is suggested to use more sensors to eliminate the possibility of some sensors being located in non-preferred directions, which could lead to non-detection or insufficient hits for location of some events. Third, to fully characterize the frequency content of the AE signals in the hybrid plate, requires sensors with similar response sensitivity to both high and low frequencies. Finally, the results of the current study demonstrate the high value of the use of FEM to gain insight before testing or to interpret experimental AE results from a composite with large changes in stiffness versus direction.

## References

[1] Markus G. R. Sause, Marvin A. Hamstad and Siegfried Horn, “Finite element modeling of lamb wave propagation in anisotropic hybrid materials,” Composites Part B: Engineering 53 (2013), pp. 249-257, doi: 10.1016/j.compositesb.2013.04.067.
[2] K. S. Downs, M. A. Hamstad and A. O’Gallagher, “Wavelet Transform Signal Processing to Distinguish Different Acoustic Emission Sources,” J. of Acoustic Emission, Vol. 21, 2003, pp. 52-69.
[3] Brian Burks and Marvin Hamstad, “The impact of solid-fluid interaction on transient stress wave propagation due to Acoustic Emissions in multilayer plate structures with applications to detection,” Brian Burks and Marvin Hamstad, submitted 2014.
[4] Xue Qi and Xiaoliang Zhao, “Ultrasonic guided wave simulation toolbox development for damage detection in composite,” AIP Conf. Proc, 1211, pp. 1095-1102, 2010. Implemented in “NDE Wave & Image Processor Software User Manual,” v3.0, D.J. Roth, 2010.
[5] Hyiung-Ill Choi and William J. Williams, “Improved time-frequency representation of multicomponent signals using exponential kernels,” IEEE Transactions on Acoustics, Speech and Signal Processing, Vol. 37, no. 6, 1989, pp. 862-871.
[6] AGU-Vallen Wavelet software, version R2010.0202, Vallen Systeme GmbH, Icking, Germany (2010). Available at http://www.vallen.de/downloads.
[7] M. A. Hamstad, A. O’Gallagher and J. Gary, “Examination of the Application of a Wavelet Transform to Acoustic Emission Signals: Part 1. Source Identification,” J. of Acoustic Emission, Vol. 20, 2002, pp. 39-61.

[8] M.A. Hamstad, unpublished, 2014.
[9] C.B. Scruby, "Quantitative Acoustic Emission Techniques," In Research Techniques in Nondestructive Testing, Chap. 4, Vol. 8, ed. R. S. Sharpe, Academic Press Inc., London, 1985, pp. 141-210.